

Tail Emission of Prompt Gamma-Ray Burst Jets

Ryo Yamazaki^{1,2*}, Kenji Toma³, Kunihiro Ioka³ and Takashi Nakamura³

¹*Department of Physics, Hiroshima University, Higashi-Hiroshima, Hiroshima 739-8526, Japan*

²*Department of Earth and Space Science, Osaka University, Toyonaka 560-0043, Japan*

³*Department of Physics, Kyoto University, Kyoto 606-8502, Japan*

19 February 2019

ABSTRACT

Tail emission of the prompt gamma-ray burst (GRB) is discussed using a multiple emitting sub-shell (inhomogeneous jet, sub-jets or mini-jets) model, where the whole GRB jet consists of many emitting sub-shells. One may expect that such a jet with angular inhomogeneity should produce spiky tail emission. However, we found that the tail is not spiky but is decaying roughly monotonically. The global decay slope of the tail is not so much affected by the local angular inhomogeneity but affected by the global sub-shell energy distribution. The fact that steepening breaks appeared in some events prefers the structured jets. If the angular size of the emitting sub-shell is around 0.01–0.02 rad, some bumps or fluctuations appear in the tail emission observed frequently in long GRBs. If the parameter differences of sub-shell properties are large, the tail has frequent changes of the temporal slope observed in a few bursts. Therefore, the multiple emitting sub-shell model has the advantage of explaining the small-scale structure in the observed rapid decay phase.

Key words: gamma rays: bursts — gamma rays: theory.

1 INTRODUCTION

Gamma-ray bursts (GRBs) consist of two phases: prompt GRB emission and subsequent afterglows. How long the prompt GRB emission lasts and when the transition from the prompt GRB to the afterglow occurs have been long-standing problems. These problems are tightly related to the mechanism of the central engine of GRBs. In general, the prompt GRB tends to show a spectral softening and a rapid decay (e.g., Giblin et al. 1999; Connaughton 2002), so that the X-ray observation with high flux sensitivity is necessary to investigate the end epoch of the prompt GRB. Such an observation has become possible thanks to the *Swift* satellite, which are revealing rich structures in early X-ray counterparts of GRBs (Burrows et al. 2005; Chincarini et al. 2005; Campana et al. 2005; Tagliaferri et al. 2005; Nousek et al. 2005; O’Brien et al. 2006). A distinct decaying component before the usual afterglow phase is identified. During this epoch, the decay is steeper and the spectral index is different compared with the subsequent phase (Nousek et al. 2005). These results suggest that this component is the tail emission of the prompt GRB (Zhang et al. 2005; Panaitescu et al. 2005).

Most natural explanation for the tail is a high latitude emission from a relativistically moving shell (Kumar & Panaitescu 2000; Yamazaki et al. 2005). Suppose

the shell shines for a short period. Since the shell has a curvature, photons far from the line of sight come later. Because the shell at higher latitude from the line of sight has a lower velocity toward the observer, the emission becomes dimmer and softer as time passes because of the relativistic beaming effect. For a spherical uniform shell, the predicted decay index, α , is related to the photon index, $\beta (< 0)$, as $\alpha = -1 + \beta$ (Kumar & Panaitescu 2000).

However, there are many difficulties when we interpret the observed prompt GRB tails with the current model in which the uniform, instantaneous emission is assumed (Kumar & Panaitescu 2000). The observed α – β relation for the steep decay phase does not tightly obey the relation, $\alpha = -1 + \beta$, but has a wide scatter. This suggests that several additional factors are needed to spread the relation. Some events showed the steepening break in the tail (O’Brien et al. 2006), which suggests the assumption of the uniform shell in the current model should be modified. Moreover, some light curves in the rapid decay phase are neither simply monotonic nor smooth, but show some bumps and dips (e.g., see Fig. 1 of Tagliaferri et al. 2005). Some bursts showed frequent changes in the temporal slope of the rapid decay phase (O’Brien et al. 2006). These small-scale features are not produced by the smooth jet with angular homogeneity. Hence we should modify the current model in order to explain these detailed observed features. Since the emission region sweeps the shell spatially, the tail emission features,

* E-mail: ryo@theo.phys.sci.hiroshima-u.ac.jp (RY)

e.g., the decay index and smoothness, would diagnose the unknown angular structure of the GRB jet.

In this paper, we study the tail emission of the prompt GRB using a multiple emitting “sub-shell” (inhomogeneous jet, sub-jets or mini-jets) model considered so far (Nakamura 2000; Kumar & Piran 2000; Yamazaki et al. 2004b; Toma et al. 2005a,b). Standard GRB scenario assumes the density fluctuation in the radial direction, and the high-density region is called the “shell”. Although the matter exists outside of the shell in general, we usually adopt the null-density approximation there. Similar to the radial direction, one can expect that the GRB outflow has the inhomogeneity also in the angular direction, because causally connected region has an angular size of γ^{-1} , which is an order of magnitude smaller than that of the GRB jet inferred from the afterglow observations. We further develop this picture and consider the emission region is patchy. We call each patch as sub-shell. Similar to null-density approximation in the shell, we assume that outside of the sub-shell, there is little emission. Therefore, multiple sub-shell approximation is along a natural extension of current standard scenario, though it is an extreme model to express the local angular inhomogeneity. One may consider our sub-shell model as a finite difference version of the continuous variable in numerical simulations. Our basic claim is that the relativistic kinematics and the viewing angle effect are one of the most important parameters that causes observed properties of GRBs. At present it is important to investigate pure kinematical effects with other parameters fixed. Our previous works have shown that multiple sub-shell model can explain the observed diversity of prompt GRB emission. *Swift* observations show the diversity of early X-ray afterglow light curves, which might be ascribed to the angular inhomogeneity of GRB jets. So far, no one has investigated the prompt GRB tail using the multiple sub-shell model, though the subsequent afterglow phase arising from external shocks with angular inhomogeneity has been calculated (e.g., Rossi et al. 2002). This paper is organized as follows. In § 2, we briefly introduce our prompt emission model. The tail emission of GRB is discussed in § 3. In § 4, we will see that our model well reproduces the observed features of the tail emission of the prompt GRB. Section 5 is devoted to discussions.

2 PROMPT EMISSION MODEL

We consider the same model as discussed in our previous works (Yamazaki et al. 2004b; Toma et al. 2005a,b). The whole GRB jet, whose opening half-angle is $\Delta\theta_{\text{tot}}$, consists of N_{tot} emitting sub-shells (sub-jets) (Nakamura 2000; Kumar & Piran 2000). We introduce the spherical coordinate system $(r, \vartheta, \varphi, t)$ in the central engine frame, where the origin is at the central engine, and $\vartheta = 0$ is the axis of the whole jet. Each sub-jet departs at time $t_{\text{dep}}^{(j)}$ ($0 < t_{\text{dep}}^{(j)} < t_{\text{dur}}$, where $j = 1, \dots, N_{\text{tot}}$, and t_{dur} is the active time of the central engine) from the central engine in the direction of $\vec{n}^{(j)} = (\vartheta^{(j)}, \varphi^{(j)})$. The direction of the observer is denoted by $\vec{n}_{\text{obs}} = (\vartheta_{\text{obs}}, \varphi_{\text{obs}})$. For each sub-jet, the emission model is the same as in the previous works (Granot et al. 1999; Woods & Loeb 1999; Ioka & Nakamura 2001; Yamazaki et al. 2002, 2003, 2004a). The observed flux from the j th sub-jet is calculated when the following pa-

rameters are determined: the viewing angle of the sub-jet $\theta_v^{(j)} = \cos^{-1}(\vec{n}_{\text{obs}} \cdot \vec{n}^{(j)})$, the opening half-angle of the sub-jet $\Delta\theta_{\text{sub}}^{(j)}$, the departure time $t_{\text{dep}}^{(j)}$, the Lorentz factor $\gamma^{(j)} = (1 - \beta_{(j)}^2)^{-1/2}$, the emitting radius $r_0^{(j)}$, the low- and high-energy photon index $\alpha_B^{(j)}$ and $\beta_B^{(j)}$, the break frequency in the shell comoving frame $\nu_0^{\prime(j)}$ (Band et al. 1993), the normalization constant of the emissivity $A^{(j)}$, and the source redshift z . The whole light curve from the GRB jet is produced by the superposition of the sub-jet emission. Throughout the paper, we neglect the cosmological effect, i.e., we set $z = 0$.

As we will see later, the local inhomogeneity in our model are almost averaged during the tail emission phase, and the global jet structure (the mean sub-jet distribution) determines overall shape of the tail. Therefore, essentially we are also studying the tail emission from the usual structured jets at the same time as the limiting case, i.e., from uniform or power-law jets with no local inhomogeneity.

3 TAIL EMISSION OF PROMPT GRB

3.1 General Kinematical Considerations

We present some of kinematical properties of prompt GRBs in the multiple sub-jet model. Let $\theta_v^{(j)}$ be the angle between the observer’s line of sight and the axis of the j th sub-jet. The pulse starting and ending time at the observer are given by

$$T_{\text{start}}^{(j)} \sim t_{\text{dep}}^{(j)} + \frac{r_0^{(j)}}{2c\gamma_{(j)}^2} \left(1 + \gamma_{(j)}^2 \theta_{-}^{(j)2}\right), \quad (1)$$

$$T_{\text{end}}^{(j)} \sim t_{\text{dep}}^{(j)} + \frac{r_0^{(j)}}{2c\gamma_{(j)}^2} \left(1 + \gamma_{(j)}^2 \theta_{+}^{(j)2}\right), \quad (2)$$

where $\theta_{+}^{(j)} = \theta_v^{(j)} + \Delta\theta_{\text{sub}}^{(j)}$ and $\theta_{-}^{(j)} = \max\{0, \theta_v^{(j)} - \Delta\theta_{\text{sub}}^{(j)}\}$, and we use the formulae $\beta_{(j)} \sim 1 - 1/2\gamma_{(j)}^2$ and $\cos\theta \sim 1 - \theta^2/2$ for $\gamma^{(j)} \gg 1$ and $\theta \ll 1$, respectively. The observer time $T = 0$ is chosen as the time of arrival at the observer of a photon emitted at the origin $r = 0$ at $t = 0$. Then, the pulse duration, $\delta T^{(j)} = T_{\text{end}}^{(j)} - T_{\text{start}}^{(j)}$, is given by $\delta T^{(j)} \sim 1.5 r_{14} (\theta_{+}^{(j)}/0.03)^2$ s for $\theta_v^{(j)} < \Delta\theta_{\text{sub}}^{(j)}$, and

$$\delta T^{(j)} \sim 26 r_{14} (\Delta\theta_{\text{sub}}^{(j)}/0.02) (\theta_v^{(j)}/0.2) \text{ sec}, \quad (3)$$

for $\theta_v^{(j)} > \Delta\theta_{\text{sub}}^{(j)}$, where $r_{14} = r_0^{(j)}/10^{14}$ cm. The peak energy $E_p^{(j)}$, that gives the peak of the νF_ν spectrum, is approximated as $E_p^{(j)} \propto \nu_0^{\prime(j)} \delta^{(j)}$, where $\delta^{(j)} = [\gamma^{(j)}(1 - \beta_{(j)} \cos\theta_{-}^{(j)})]^{-1}$. Using practical numerical calculations, we find $E_p^{(j)} \sim 6.5 \times 10^2 \gamma_2 \nu_5$ keV for $\theta_v^{(j)} \ll \Delta\theta_{\text{sub}}^{(j)}$, and

$$E_p^{(j)} \sim 2 \gamma_2^{-1} \nu_5 (\theta_v^{(j)}/0.2)^{-2} \text{ keV}, \quad (4)$$

for $\theta_v^{(j)} \gg \Delta\theta_{\text{sub}}^{(j)}$, where $\nu_5 = \nu_0^{\prime(j)}/5$ keV and $\gamma_2 = \gamma^{(j)}/10^2$ (see also Graziani et al. 2006). We note that the light curve from a single pulse becomes dim and smooth for large $\theta_v^{(j)}$ (see Fig. 2 of Ioka & Nakamura 2001).

For sub-jets with $\theta_v^{(j)} \lesssim \Delta\theta_{\text{sub}}^{(j)}$, we have $\delta T^{(j)} \ll t_{\text{dur}}$, because t_{dur} is about several tens of seconds. Then the bright pulses arising from these sub-jets are concentrated in the epoch $0 \lesssim T \lesssim t_{\text{dur}}$. On the other hand, for sub-jets with $\theta_v^{(j)} \gtrsim 0.1 r_{14}^{-1/2} (t_{\text{dep}}^{(j)}/20 \text{ sec})^{1/2}$, the second terms of the right hand sides of Eqs. (1) and (2) become larger than the first ones, so that $T_{\text{start}}^{(j)}$ and $T_{\text{end}}^{(j)}$ may be much larger than

t_{dur} for large $\theta_v^{(j)}$. Such smooth, long-duration, dim, and soft pulses make the tail emission of the prompt GRB.

Now we concentrate on the temporal structure of the tail emission. We assume that each sub-jet is not drastically different. Since $T_{\text{start}}^{(j)}$ and $T_{\text{end}}^{(j)}$ are much larger than t_{dur} , they are not affected by $t_{\text{dep}}^{(j)}$. Thus we may consider that all the sub-jets contributing to the tail emission emit simultaneously at a mean radius r_0 in the central engine frame. The end of the tail emission T_{tail} is determined by the angular size of the whole jet:

$$\begin{aligned} T_{\text{tail}} &\sim (r_0/2c)(\Delta\theta_{\text{tot}} + \vartheta_{\text{obs}})^2 \\ &\sim 2 \times 10^2 r_{14} [(\Delta\theta_{\text{tot}} + \vartheta_{\text{obs}})/0.3]^2 \text{ sec} . \end{aligned} \quad (5)$$

The tail flux at an observer time T is the superposition of the sub-jet emission with the pulse starting and ending time $T_{\text{start}}^{(j)} < T < T_{\text{end}}^{(j)}$. Sub-jets with viewing angles between $\theta_T - \Delta\theta_{\text{sub}}$ and $\theta_T + \Delta\theta_{\text{sub}}$ contribute to the tail flux at a time T , where $\theta_T = (2cT/r_0)^{1/2} \sim 0.2r_{14}^{-1/2}(T/10^2\text{s})^{1/2}$ rad. Then we may calculate the number of these contributing sub-jets $N_{\text{sub}}(T)$ and its variance $1/\sqrt{N_{\text{sub}}(T)}$ if the sub-jet distribution and observer's line of sight are given. Since $N_{\text{sub}}(T)$ is sufficiently large, the tail light curve will be smooth. In the following, we actually compute the light curves of prompt GRB emission for various cases.

3.2 Example 1: Uniform jet

We first consider the uniformly distributed sub-jets. The number of sub-jets per unit solid angle is approximately given by $dN/d\Omega = N_{\text{tot}}/(\pi\Delta\theta_{\text{tot}}^2)$ for $\vartheta < \Delta\theta_{\text{tot}}$, where $\Delta\theta_{\text{tot}} = 0.25$ rad is adopted. The departure time of each sub-jet $t_{\text{dep}}^{(j)}$ is assumed to be homogeneously random between $t = 0$ and $t = t_{\text{dur}} = 20$ sec. The central engine is assumed to produce $N_{\text{tot}} = 1000$ sub-jets. In this section, we assume that all the sub-jets have the same values of the following fiducial parameters: $\Delta\theta_{\text{sub}} = 0.02$ rad, $\gamma = 100$, $r_0 = 1.0 \times 10^{14}$ cm, $\alpha_B = -1$, $\beta_B = -2.3$, $h\nu'_0 = 5$ keV, and $A = \text{const}$.

Figure 1 shows the results, where $\vartheta_{\text{obs}} = 0$ (thick-solid line), $\Delta\theta_{\text{tot}}/2$ (dashed), $\Delta\theta_{\text{tot}}$ (dotted), and $3\Delta\theta_{\text{tot}}/2$ (dot-dashed) are considered. One can see the entire behavior of bursts in the left panel of the figure. For the cases $\vartheta_{\text{obs}} < \Delta\theta_{\text{tot}}$, as expected, the bright pulses are observed in the period $0 \lesssim T \lesssim t_{\text{dur}} = 20$ sec, and subsequently the tail emission starts. However, when $\vartheta_{\text{obs}} = 3\Delta\theta_{\text{tot}}/2$, the whole jet is seen off-axis. Then the emission becomes dim and soft (Yamazaki et al. 2002, 2003, 2004a,b). In any cases, the tail emission is smooth. For $\vartheta_{\text{obs}} = 0$, the number of contributing sub-jets $N_{\text{sub}}(T)$ is approximately given by $N_{\text{sub}}(T) \sim 4\pi\theta_T\Delta\theta_{\text{sub}}(dN/d\Omega)$. For our adopted parameters, we derive $N_{\text{sub}}(T) \sim 2.6 \times 10^2 (T/10^2\text{s})^{1/2} \gg 1$, so that the tail light curve is smooth. Also in other cases ($\vartheta_{\text{obs}} \neq 0$), we obtain $N_{\text{sub}}(T) \gg 1$.

The decay index of the tail emission, α , is about -4 when it is determined by the whole light curve (see Fig 1). The effect of choosing the zero of time is essential in order to determine α (Chincarini et al. 2005; Zhang et al. 2005). Figure 2 shows the same light curves as in Fig. 1 but the time zero is shifted to the maximum of the last bright pulse. Then, we find $-3 \lesssim \alpha \lesssim -2$. Since we may consider that all the sub-jets emit simultaneously in the central engine frame for

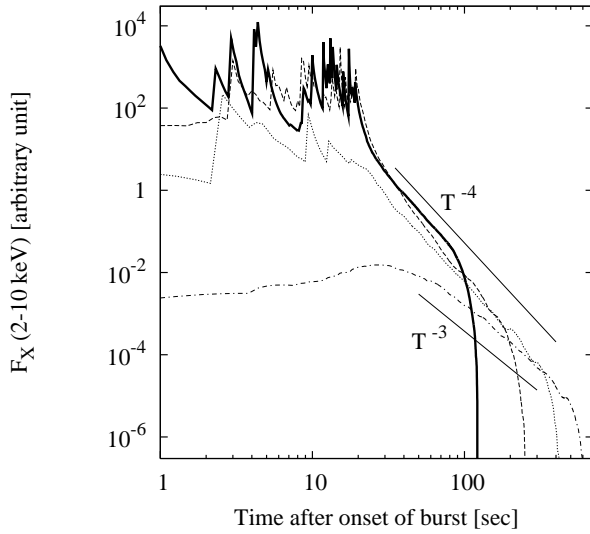


Figure 1. Examples of light curves of the prompt GRB emission calculated by the multiple emitting sub-shell model (multiple sub-jet model). The sub-jets are distributed uniformly. All sub-jets have the same intrinsic properties. Thick-solid, dashed, dotted, and dot-dashed lines correspond to the viewing angles of $\vartheta_{\text{obs}} = 0$, $\Delta\theta_{\text{tot}}/2$, $\Delta\theta_{\text{tot}}$, and $3\Delta\theta_{\text{tot}}/2$, respectively. The observer time is the time since the onset of the burst.

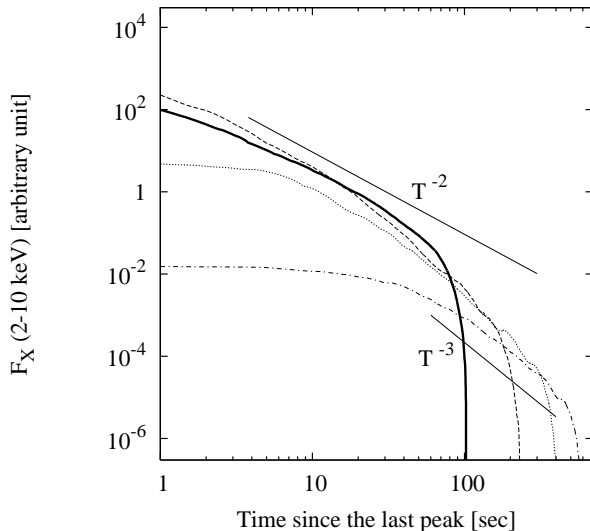


Figure 2. The same as Fig. 1, but the observer time is the time since the last bright peak.

the tail emission, the behavior of the emission may be similar for a single, spherical, infinitesimally thin shell case. Then $\alpha = -1 + \beta_B = -3.3$ is expected (Kumar & Panaitescu 2000), which is intermediate between those shown in Figures 1 and 2. This implies that the zero of time which gives us $\alpha = -1 + \beta_B$ lies between the onset of the burst and the last bright pulse. Therefore, it is difficult to check whether the relation $\alpha = -1 + \beta_B$ is satisfied or not.

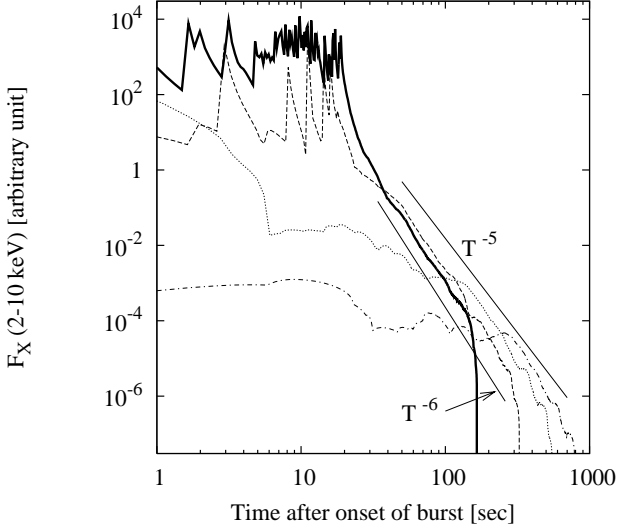


Figure 3. The same as Fig. 1 but for the power-law sub-jet distribution.

3.3 Example 2: Power-law jet

Next we consider the power-law sub-jet distribution, i.e., $dN/d\Omega = C$ for $0 < \vartheta < \vartheta_c$ and $dN/d\Omega = C(\vartheta/\vartheta_c)^{-2}$ for $\vartheta_c < \vartheta < \Delta\theta_{\text{tot}}$, where $\vartheta_c = 0.03$ rad and $\Delta\theta_{\text{tot}} = 0.3$ rad, and $C = (N_{\text{tot}}/\pi\vartheta_c^2)[1 + 2\ln(\Delta\theta_{\text{tot}}/\vartheta_c)]^{-1}$ is the normalization constant (Rossi et al. 2002; Zhang & Mészáros 2002; Toma et al. 2005a,b). The departure time of each sub-jet $t_{\text{dep}}^{(j)}$ is assumed to be homogeneously random between $t = 0$ and $t = t_{\text{dur}} = 20$ sec and we adopt $N_{\text{tot}} = 350$. We assume that all the sub-jets have the fiducial parameters.

Figures 3 and 4 show the results. Compared with the uniform jet case, the decay is steeper because the power-law jet is dimmer in the outer region, i.e., the sub-jets are sparsely distributed near the periphery of the whole jet. For example, when $\vartheta_{\text{obs}} = 0$, the number of contributing sub-jets $N_{\text{sub}}(T)$ is calculated as $N_{\text{sub}}(T) \sim 4\pi\theta_T\Delta\theta_{\text{sub}}(dN/d\Omega) \sim 28(T/10^2\text{s})^{-1/2}$, which is a decreasing function of time contrary to the uniform jet case.

4 COMPARISON BETWEEN THEORETICAL AND OBSERVATIONAL RESULTS

As can be seen in Fig. 4, a steepening break (from $\alpha \sim -1$ to $\alpha \sim -4$) occurs at about 35 sec and 100 sec after the last brightest pulse for $\vartheta_{\text{obs}} = \Delta\theta_{\text{tot}}/2$ and $\vartheta_{\text{obs}} = \Delta\theta_{\text{tot}}$, respectively. This is because the power-law jet has a core region ($0 < \vartheta < \vartheta_c$), where sub-jets densely distributed compared with the outer region. Before photons emitted by the core arrive at the observer (i.e., $\theta_T \lesssim \vartheta_{\text{obs}}$), $N_{\text{sub}}(T)$ increases with T more rapidly than in the case of the uniform sub-jet distribution. Then, the light curve shows a shallow decay or even shows a rising part. After the photons arising from the core are observed, the sub-jet emission with viewing angles larger than $\sim \vartheta_c$ is observed. Then $N_{\text{sub}}(T)$ rapidly decreases with T and the observed flux suddenly drops. Therefore, a steepening break occurs at $\theta_T \sim \vartheta_{\text{obs}}$. *Swift* observations have shown that some bursts (e.g. GRB 050421, 050713B) have

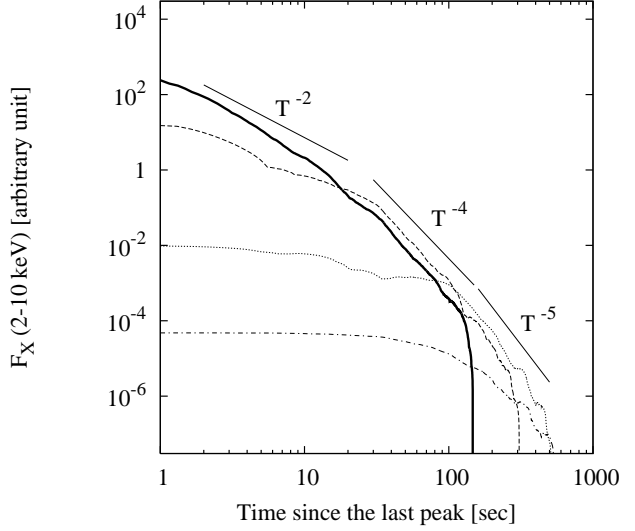


Figure 4. The same as Fig. 2 but for the power-law sub-jet distribution.

the steepening break, which may support the structured jet case.

Observed rapid decay phase lasts at least ~ 100 sec in the cosmological rest frame (Nousek et al. 2005), which constrains the emitting radius r_0 . As can be seen in Fig. 5, when r_0 is small (the thin-solid line) the tail emission ends rapidly, while the end time of the tail emission, T_{tail} , does not depend on $\Delta\theta_{\text{sub}}$ and γ [see Eq. (5)]. The end time of the tail is difficult to be determined because the subsequent shallow decay arising from the external shock overlies the prompt tail emission. So, we can set $T_{\text{tail}} \gtrsim 10^2$ sec, and obtain $r_0 \gtrsim 5 \times 10^{13} [(\Delta\theta_{\text{tot}} + \vartheta_{\text{obs}})/0.3]^{-2}$ cm.

Observed light curves in a rapid decay phase are neither simply monotonic nor smooth, but show some bumps and dips (e.g., see Fig. 1 of Tagliaferri et al. 2005). These small-scale features are not explained by the angularly continuous jet model. We claim that they come from the inhomogeneity of the emission region. In calculating the light curves shown in Figs. 1–4, we assumed $\Delta\theta_{\text{sub}} = 0.02$ rad, so that the local inhomogeneity was erased and smooth monotonic decay behavior appeared. If $\Delta\theta_{\text{sub}}$ becomes small, we can obtain the light curve with small bumps similar to the observed one. Figure 5 shows the dependence on the assumed parameters on $\Delta\theta_{\text{sub}}$ and γ (but still the same for all j), where we fix the observer's line of sight $\vartheta_{\text{obs}} = 0$ and the power-law sub-jet distribution is considered. When $\Delta\theta_{\text{sub}}$ is small (dotted and dot-dashed lines), $\delta T^{(j)}$ is small [see Eq. (3)], so that $N_{\text{sub}}(T)$ decreases. Then the observed light curves remarkably reflect fluctuations of $N_{\text{sub}}(T)$. On the other hand, when γ is large but other parameters are fixed (dashed and dot-dashed lines), the smoothness of the light curve remains unchanged because $N_{\text{sub}}(T)$ does not depend on γ . Then, the asymptotic decay slope is unchanged, though the flux becomes dim for large γ because the relativistic beaming effect is large.

Some bursts showed frequent changes in a temporal slope of the rapid decay phase (O'Brien et al. 2006). For example, GRB 050819 exhibited steep decay with small fluctu-

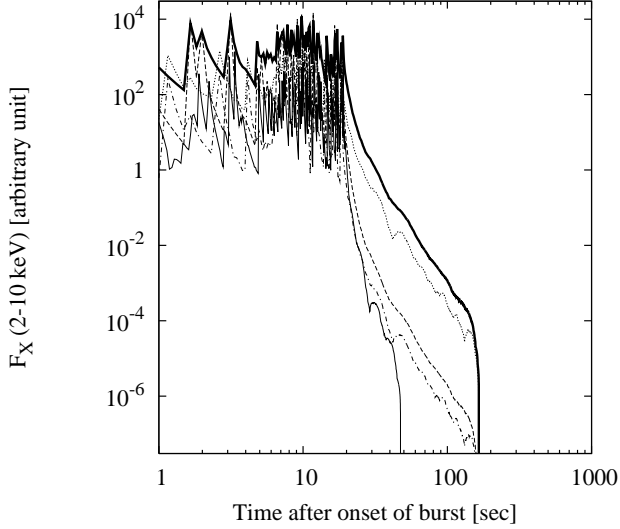


Figure 5. Comparison of light curves with different parameter sets of $\Delta\theta_{\text{sub}}$, γ , and r_0 for the power-law distribution. Dashed ($\gamma = 400$), dotted ($\Delta\theta_{\text{sub}} = 0.01$ rad), dot-dashed ($\gamma = 400$ and $\Delta\theta_{\text{sub}} = 0.01$ rad), and thin-solid lines ($r_0 = 0.2 \times 10^{14}$ cm) with the other parameters being fiducial, i.e., $\Delta\theta_{\text{sub}} = 0.02$ rad, $\gamma = 100$, and $r_0 = 1.0 \times 10^{14}$ cm. The thick-solid line is the same as that in Fig. 3 (fiducial set). All lines have $\vartheta_{\text{obs}} = 0$.

ations until ~ 250 sec after the BAT trigger. Subsequently, the decay became shallow and lasted for ~ 250 sec, and the rapidly decaying tail started again at ~ 500 sec after the BAT trigger. We find that when the differences of sub-jet properties are small, such observed behavior does not appear. In Fig. 6, the value of $\gamma\nu_0^{(j)}$ is distributed randomly according to the log-normal distribution with an average of $\log(350 \text{ keV})$ and a logarithmic variance of 0.2, and $A^{(j)}$ is determined so that the observed flux is proportional to ξE_p^2 for $\theta_v^{(j)} = 0$, where ξ is also assumed to obey a log-normal distribution with a logarithmic variance of 0.15 (Lloyd-Ronning & Ramirez-Ruiz 2002; Yonetoku et al. 2004; Liang et al. 2004). When the variance is small (dashed and dotted lines), the change of the slope is small, while the shape is similar to that of GRB 050819 for larger variance case (dot-dashed line). However, the small number of events showing such complicated decay behavior like GRB 050819 may suggest that the differences of sub-jet properties are small.

5 DISCUSSION

We have examined the tail emission of the prompt GRB in the X-ray band using a multiple emitting sub-shell (inhomogeneous jet, sub-jets or mini-jets) model, and have confirmed that our inhomogeneous jet model well reproduces the observed features of the tail emission. The sub-shell emission with a large viewing angle causes a smooth, long-duration, dim, soft pulse and arrives later than the bright hard spikes. These components make the tail emission of the prompt GRB similar to the observed one. Since the pulse duration is long for a large viewing angle, the local inhomogeneity

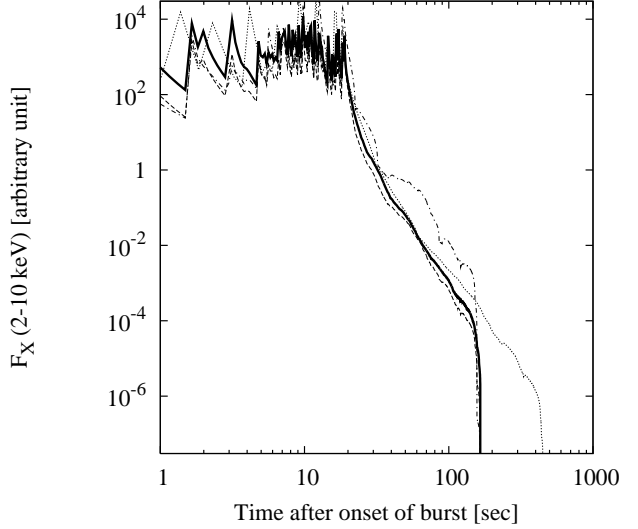


Figure 6. Comparison of light curves with different parameter sets of $\Delta\theta_{\text{sub}}$, γ , and r_0 for the power-law distribution. The value of $\gamma\nu_0^{(j)}$ is distributed randomly according to the log-normal distribution with an average of $\log(350 \text{ keV})$ and a logarithmic variance of 0.2, and $A^{(j)}$ is determined so that the observed flux is proportional to ξE_p^2 for $\theta_v^{(j)} = 0$, where ξ is also assumed to obey a log-normal distribution with a logarithmic variance of 0.15 (Lloyd-Ronning & Ramirez-Ruiz 2002; Yonetoku et al. 2004; Liang et al. 2004). The dashed line corresponds to the fiducial parameter set of $\Delta\theta_{\text{sub}}$, γ , and r_0 , while the dotted line is for $\gamma = 300$ and $r_0 = 3.0 \times 10^{14}$ cm. The dot-dashed line is for the case in which logarithmic variance of $\gamma\nu_0^{(j)}$ is changed into 0.8. The thick-solid line is the same as that in Fig. 3 (fiducial set). All lines have $\vartheta_{\text{obs}} = 0$.

is almost averaged and the continuous light curve is obtained. The global sub-jet angular distribution determines the shape of the global decay slope of the tail. Therefore, the discrete multiple sub-jet model and the continuous surface model obtained by averaging sub-jets predict the same “averaged” decay index. We have found that the decay is steeper for the power-law jet case than for the uniform jet case. It has been also found that if there is a core, in which many emitting shells exist compared with other regions, the steepening break appears in the tail when the core is viewed off-axis. Such steepening breaks have been seen for some bursts. Finally, it has been found that in the sub-jet model with $\Delta\theta_{\text{sub}} \sim 0.01$ rad, the local inhomogeneity is not entirely erased in the tail and makes small bumps or fluctuations on the smooth decay that have been observed in many events.

Swift observation has revealed the short-duration and large-amplitude flares in some X-ray afterglows (Burrows et al. 2005). Such X-ray flares during the afterglow phase are thought to be produced by the long-acting engine (Ioka et al. 2005). In our multiple sub-shell model, when a sub-shell causes very bright emission with large viewing angle, the flare-like structure is observed in the rapid decay phase. Hence the X-ray flare in the rapid decay phase may be originated in either the long-acting engine or the angular inhomogeneity of the emitting jet.

For uniform, instantaneous emission, the decay index,

α , of the prompt GRB tail is related to the photon index, β , as $\alpha = -1 + \beta$ (Kumar & Panaitescu 2000). As seen in this paper, there are several effects that make the decay index different from this simple relation: choosing the time zero, the energy distribution of the jet, and the viewing angle of the jet. It is difficult to separate these factors from the observation. Therefore, the observed α - β relation would have a wide scatter.

A typical value of the viewing angle at an observer time T is $\theta_T \sim 0.2(T/10^2\text{s})^{1/2}$ rad, and then the peak energy, E_p , is about a few keV [see Eq. (4)]. Therefore, the spectral index in the X-ray band is given by the high-energy photon index $\beta_B \sim -2.3$, which is consistent with the observed photon index that ranges between 1.34 and 3.25 (average value is 2.28) (Nousek et al. 2005).

Important parameters that characterize our model are the number of sub-jets N_{tot} and the opening half-angle of the sub-jet $\Delta\theta_{\text{sub}}$. Given the sub-jet angular distribution, the value of N_{tot} is determined in order to reproduce the number of sub-jets along a line of sight, n_s , that ranges between about 10 and 10^2 because n_s corresponds to the number of bright pulses observed in usual long GRBs (Yamazaki et al. 2004b). In our adopted parameters, the maximum of n_s is about 10 and 30 for uniform jet case and the power-law jet case, respectively. On the other hand, the value of $\Delta\theta_{\text{sub}}$ has been fairly uncertain. It is a common sense that $\Delta\theta_{\text{sub}}$ is larger than γ^{-1} because even if $\Delta\theta_{\text{sub}} \ll \gamma^{-1}$ initially, jet expands sideways and the asymptotic value of $\Delta\theta_{\text{sub}}$ is γ^{-1} . However, in principle, $\Delta\theta_{\text{sub}}$ could be even smaller than γ^{-1} e.g., if the offset collision of two shells is considered. In this paper, we have found that the most preferable is the case of $\Delta\theta_{\text{sub}} \sim \gamma^{-1} \sim 0.01$ rad. If $\Delta\theta_{\text{sub}} \ll 0.01$, the tail would be so spiky, while if $\Delta\theta_{\text{sub}} \gg 0.01$, the tail would be so smooth that small-scale bumps would disappear.

The behavior of afterglow light curves of GRBs may also be a diagnostic tool to investigate the jet structure (Rossi et al. 2002; Granot & Kumar 2003; Panaitescu & Kumar 2003). However, the prompt GRB tail is better than the afterglow light curve for this purpose. This is because the information of the jet structure is lost at later time due to the hydrodynamical energy re-distribution effect (Granot & Kumar 2003) and the tail emission reflects the GRB jet structure more directly.

ACKNOWLEDGMENTS

We would like to thank the anonymous referee, T. Sakamoto, G. Sato, T. Takahashi, and D. Yonetoku for useful comments and discussions. This work was supported in part by Grants-in-Aid for Scientific Research of the Japanese Ministry of Education, Culture, Sports, Science, and Technology 09245 (R. Y.), 14047212 (T. N., K. I.), 14204024 (T. N.), and 17340075 (T. N.).

REFERENCES

Band D. L. et al., 1993, ApJ, 413, 281
 Burrows D. N. et al., 2005, Science, 309, 1833
 Campana S. et al., 2005, ApJ, 625, L23
 Chincarini G. et al., 2005, astro-ph/0506453

Connaughton V., 2002, ApJ, 567, 1028
 Giblin T. W. et al., 1999, ApJ, 524, L47
 Granot J., Kumar, P., 2003, ApJ, 591, 1086
 Granot J., Piran T., Sari R., 1999, ApJ, 513, 679
 Graziani C., Lamb D. Q., Donaghy T. Q., 2006, astro-ph/0505623
 Ioka K., Kobayashi S., Zhang B., 2005, ApJ, 631, 429
 Ioka K., Nakamura T., 2001, ApJ, 554, L163
 Kumar P., Panaitescu A., 2000, ApJ, 541, L51
 Kumar P., Piran T., 2000, ApJ, 535, 152
 Liang E. W., Dai Z. G., Wu X. F., 2004, ApJ, 606, L29
 Lloyd-Ronning N. M., Ramirez-Ruiz E., 2002, ApJ, 576, 101
 Nakamura T., 2000, ApJ, 534, L159
 Nousek J. A. et al., 2005, astro-ph/0508332
 O'Brien P. T. et al., 2006, astro-ph/0601125
 Panaitescu A., Kumar, P., 2003, ApJ, 592, 390
 Panaitescu A., Mészáros P., Gehrels N., Burrows D., Nousek J., 2005, astro-ph/0508340
 Rossi E., Lazzati D., Rees M. J., 2002, MNRAS, 332, 945
 Tagliaferri G. et al., 2005, Nat, 436, 985
 Toma K., Yamazaki R., Nakamura T., 2005a, ApJ, 620, 835
 Toma K., Yamazaki R., Nakamura T., 2005b, ApJ, 635, 481
 Woods E., Loeb A., 1999, ApJ, 523, 187
 Yamazaki R., Ioka K., Nakamura T., 2002, ApJ, 571, L31
 Yamazaki R., Ioka K., Nakamura T., 2003, ApJ, 593, 941
 Yamazaki R., Ioka K., Nakamura T., 2004a, ApJ, 606, L33
 Yamazaki R., Ioka K., Nakamura T., 2004b, ApJ, 607, L103
 Yamazaki R., Ioka K., Takahara F., Shibazaki N., 2005, PASJ, 57, L11
 Yonetoku D., Murakami T., Nakamura T., Yamazaki R., Inoue A. K., Ioka K., 2004, ApJ, 609, 935
 Zhang B., Mészáros P., 2002, ApJ, 571, 876
 Zhang B. et al., 2005, astro-ph/0508321